Sedimentology (2005) **52,** 1343–1359 doi: 10.1111/j.1365-3091.2005.00748.x

On the transition between 2D and 3D dunes

JEREMY G. VENDITTI*[1], MICHAEL CHURCH* and SEAN J. BENNETT†
*Department of Geography, University of British Columbia, Vancouver, BC, Canada V6T 1Z2 (E-mail: jgvenditti@yahoo.ca)
†Department of Geography, University at Buffalo, Buffalo, NY 14261-0055, USA

ABSTRACT

Sediment transport in sand-bedded alluvial channels is strongly conditioned by bedforms, the planimetric morphology of which can be either two- or three-dimensional. Experiments were undertaken to examine the processes that transform the bed configuration from two-dimensional (2D) dunes to three-dimensional (3D) dunes. A narrowly graded, 500 μm size sand was subjected to a 0·15 m deep, non-varying mean flow ranging from 0·30 to 0·55 m sec^{-1} in a 1 m wide flume. Changes in the planimetric configuration of the bed were monitored using a high-resolution video camera that produced a series of 10 sec time-lapsed digital images. Image analysis was used to define a critical value of the non-dimensional span (sinuosity) of the bedform crestlines that divides 2D forms from 3D forms. Significant variation in the non-dimensional span is observed that cannot be linked to properties of the flow or bedforms and thus appears random. Images also reveal that, once 2D bedforms are established, minor, transient excesses or deficiencies of sand are passed from one bedform to another. The bedform field appears capable of absorbing a small number of such defects but, as the number grows with time, the resulting morphological perturbations produce a transition in bed state to 3D forms that continue to evolve, but are pattern-stable. The 3D pattern is maintained by the constant rearrangement of crestlines through lobe extension and starving downstream bedforms of sediment, which leads to bifurcation. The experiments demonstrate that 2D bedforms are not stable in this calibre sand and call into question the reliability of bedform phase diagrams that use crestline shape as a discriminator.

Keywords 3D bedforms, dunes, fluvial processes, ripples, sediment transport.

INTRODUCTION

Observations in rivers and flumes within the past 50 years have revealed that in flows over sand beds a typical sequence of bedforms evolves as the velocity increases (e.g. Simons *et al.*, 1961; Guy *et al.*, 1966; Simons & Richardson, 1966). This continuum of bedforms is conceived to occur under a graduated set of flow regimes and includes lower regime bedforms (lower stage plane bed–ripples–dunes) and upper regime bedforms (upper stage plane bed–antidunes–chute-pool). The planimetric morphology of fully developed ripples and dunes can be divided into two subclasses: two-dimensional (2D) and three-dimensional (3D) bedforms. Two-dimensional ripples and dunes have fairly regular spacing, heights and lengths. Their crestlines tend to be straight or slightly sinuous and are oriented perpendicular to the mean flow lines. In contrast, 3D features have irregular spacing, heights and lengths, with highly sinuous or discontinuous crestlines (Ashley, 1990).

Most research on small-scale bedforms suggests that, under low flow conditions, bedforms exhibiting a 2D straight-crested morphology are common and, at higher flow velocities, 3D forms are established, exhibiting linguoid shapes (Fig. 1;

[1]Present address: Department of Earth and Planetary Sciences, University of California, Berkeley, CA, 94720, USA.

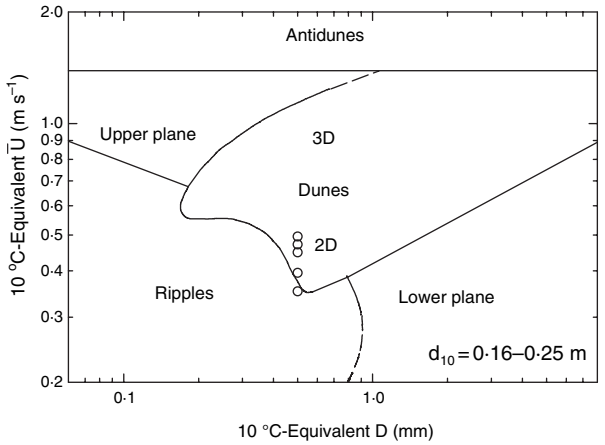

Fig. 1. Bedform phase diagram after Southard & Boguchwal (1990). The mean velocity $\bar{U}$, flow depth d and grain size D have been adjusted to their 10 °C equivalent using the methods in Southard & Boguchwal (1990). Open circles are the runs discussed in this paper.

Southard & Boguchwal, 1990; Southard, 1992). The time required to form each morphology is relatively short (tens of minutes to hours) in both circumstances (Southard, 1992). Several authors have also argued that 2D bedforms form under 2D flow conditions while 3D bedforms occur when the flow is 3D (e.g. Allen, 1968; Costello & Southard, 1981; Ashley, 1990; Southard & Boguchwal, 1990; Southard, 1992). Explicit assumptions have been made that 2D bedforms are in equilibrium with the flow over them and that there is some change in the flow structure at higher velocities that triggers change in the bedforms.

The assumption that 2D bedforms are in equilibrium arises from classical conceptions of bedform stability and the nature of the experiments that have defined this stability. Classical concepts of a continuum of bedforms assume that transitions among lower regime plane beds, ripples, dunes and upper regime plane beds are sharp. In many cases, transitions occur within an increase of a few centimetres per second in flow velocity. The transition between 2D and 3D bedforms is envisioned to occur in much the same way, despite the fact that the transition is not sharp (Costello & Southard, 1981).

Seminal work by Baas and collaborators (Baas *et al.*, 1993; Baas, 1994, 1999) contradicts this concept. They showed that, although 2D ripples often appear to be in equilibrium, given enough time will develop into 3D linguoid ripples. The time required for this transition to occur may be several days in some cases. In spite of this work, the processes that transform a 2D bedform field into 3D forms are not well understood. Furthermore, an understanding of how the planimetric morphology of a bedform field changes with time has not been examined. A bedform field will surely undergo changes in its 3D qualities, becoming more or less 3D at certain times. There is currently no way to quantify this possibility or any understanding of why a bed remains 3D once it has achieved this morphology.

The phenomenological study presented here builds on the work of Baas and collaborators by: (i) determining if the ripple plan model of Bass and collaborators is valid for dune bedforms, (ii) establishing a quantitative measure of bedform three-dimensionality, (iii) investigating its variation during bedform development and migration, (iv) determining how the transition between 2D and 3D bedforms is initiated, and (v) examining how a 3D bed morphology is maintained through time.

EXPERIMENTAL METHODOLOGY

The experiments were conducted at the National Sedimentation Laboratory, United States Department of Agriculture, in Oxford, Mississippi, using a tilting recirculating flume 15·2 m long, 1 m wide, and 0·30 m deep. The flume was filled with *ca* 2250 kg (5000 lbs) of washed and sieved white quartz sand with a median grain size diameter D_{50} of 0·500 mm. There was no sediment outside the 0·355–0·710 mm size range.

Bedform development was observed over five separate flow stages (referred to as flows A to E; Table 1) during 12 h runs. Flow depth d was *ca* 0·15 m and mean flow velocities $\bar{U}$ ranged between 0·35 and 0·50 m sec^{-1}. Froude and Reynolds numbers indicate that the flow was both sub-critical and fully turbulent (see Table 1). These five flow stages were selected to provide a test of similarity among the observations over a range of hydraulic conditions.

Bedforms developed instantaneously from a flat sand bed over the entire bed surface (from the head box to tail box) at flows A, B and C while at flows D and E, bedforms were initiated from artificial defects placed in the otherwise flat bed. These beds remained flat without the defects (Venditti *et al.*, 2005). Bed surface topography was digitized using two acoustic echo-sounders built by the National Center for Physical Acoustics (NCPA) at the University of Mississippi. The sensors had a nominal resolution that was much

Table 1. Summary of initial flow parameters and equilibrium bedform dimensions.

Flow parameter	Flow A	Flow B	Flow C	Flow D	Flow E
d, m	0·152	0·152	0·153	0·153	0·153
$\bar{U}$, m sec^{-1}	0·501	0·477	0·454	0·399	0·356
Fr	0·411	0·391	0·370	0·326	0·290
Re	75 936	72 331	69 568	61 093	54 580
Q, m^3 sec^{-1}	0·0759	0·0723	0·0696	0·0611	0·0546
$S\times10^{-4}$	12	11	7·0	5·5	5·5
Determinations based on Law of the Wall using lower 20% of velocity profiles					
u_*, m sec^{-1}	0·030	0·026	0·022	0·017	0·016
τ, Pa	0·902	0·650	0·481	0·291	0·242
Re_g	15	13	11	9	8
ff	0·029	0·023	0·019	0·015	0·015
Average equilibrium bedform dimensions					
$\bar{H}_e$, mm	47·70	41·61	35·88	21·52	19·67
$\bar{L}_e$, m	1·172	0·860	0·954	0·383	0·300
$\bar{R}_e$ mm sec^{-1}	0·650	0·371	0·334	0·172	0·097
$\overline{NDS}_{im}$	1·3422	1·3971	1·3355	1·4256	1·3986

Velocity data are derived from measurements taken with a 300 mW Dantec Laser Doppler Anemometer (see Venditti, 2003 for details).
$Fr = \bar{U}/(gd)^{0.5}$; $Re = d\bar{U}/\nu$, $ff = 8\tau/\rho\bar{U}^2$, $u_* = (\tau/\rho)^{0.5}$, $Re_g = Du_*/\nu$. $\bar{H}_e$, $\bar{L}_e$ and $\bar{R}_e$ are based on echo-soundings.

greater than the grain size in the experiments, which was their practical resolution. The sensors were mounted in the centre of the channel with a streamwise separation of 0·133 m at *ca* 10·50 m from the head box and sampled at 4 Hz.

The development of the sand bed was monitored using a high resolution (S-VHS) video camera mounted above the flume and centred at *ca* 10·3 m from the head box. The video was focused to capture an area 1 m^2 but the length of the flume captured was 1·33 times the width. The video was illuminated with four 100 W floodlights mounted on the flume sidewalls and oriented to intersect at the camera focal point. The side lighting produced a glare-free image with light shadows that highlighted millimetre-scale changes in the bed structure. The video records were sub-sampled from the tapes using a frame grabber at an interval of 10 sec. This produced series of images that were further analysed to determine morphologic changes in the sand bed over time. All measurements were made with respect to the overhung grid in the video view. Because of the distortion caused by the distance between the grid height and the bed height, all areas measured from the images were corrected by multiplying by 1·28 and all lengths were corrected by multiplying by 1·15 (see Venditti, 2003). All measurements presented herein are based on analysis of these images, unless data are specifically attributed to the echo-soundings.

In order to examine the morphology of the bed, the video image series were analysed using a GIS software package. Figure 2 details the measurements made. To calculate an areally averaged bedform length, L_a,= A_b/y_b, the area between two crestlines A_b was digitized and the distance that the bedform extended across the flume y_b was measured along the cross-stream axis of the flume. A_b could be digitized only when both crestlines were visible in the video view and within *ca* 1·2 m of each other, placing a practical limit on L_a. Another set of measurements consisted of the length along the bedform crest L_c and a measurement of the linear distance between the end points of the crestline L_y which was measured according to the orientation of the bedform crestline. In most cases, $y_b < L_y$ although, during the 2D bedform phase, these values were nearly identical because crestlines were approximately perpendicular to the flume walls. Bedform migration rates were measured by finding the distance of movement of a crestline between two successive images separated by 60, 300 or 600 sec. Migration rates were measured at up to nine equally spaced positions across each dune crest.

BEDFORM EVOLUTION AND PLANIMETRIC MORPHOLOGY

Although the bedform fields were all initiated as 2D features, there was an eventual transition to 3D forms in all the experimental runs. This is interesting because most bedform phase diagrams that distinguish between 2D and 3D bedforms

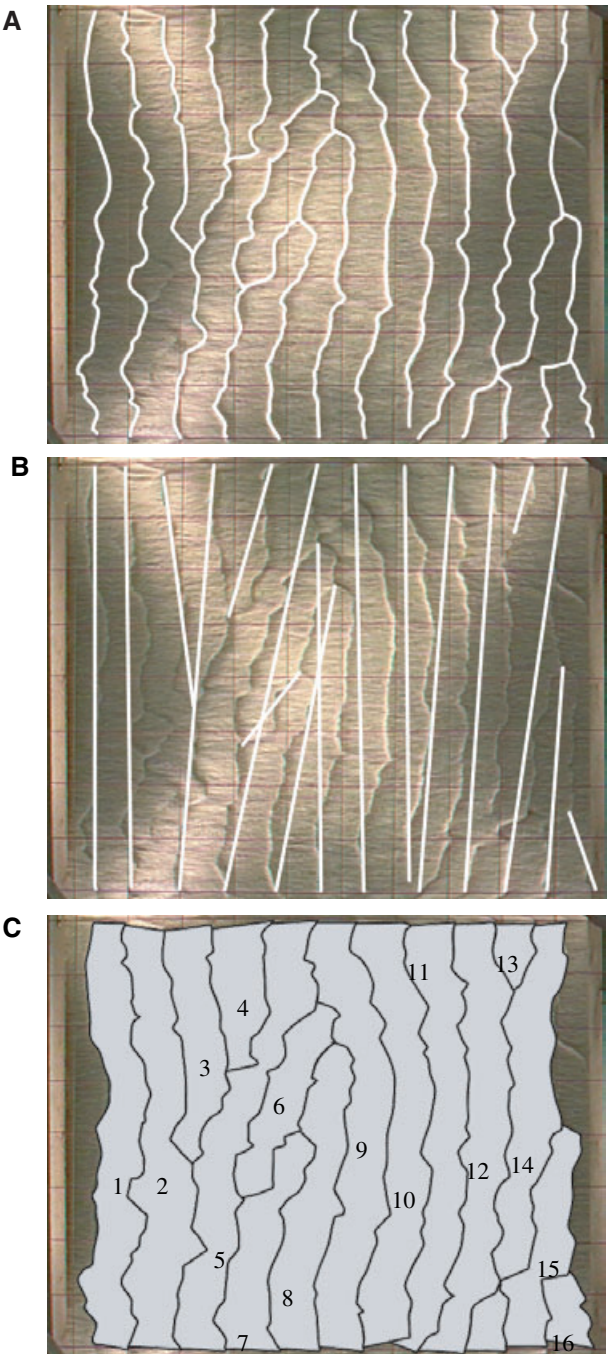

Fig. 2. Measurements taken from video images: (A) crestline length L_c; (B) linear crest length L_y; (C) bedform area A_d. Image is from flow B at $t = 240$ sec. Grid spacing is 0·115 m and flow is from left to right.

indicate that 2D forms should occur under the hydraulic conditions used here. Southard & Boguchwal (1990) have provided the most extensive bedform phase diagrams and plotting methodology in the literature to date. All the observations made during the present experiments plot in the 2D dune field of Southard & Boguchwal (1990) (Fig. 1). This result supports the work of Baas and collaborators (Baas *et al.*, 1993; Baas, 1994, 1999) by demonstrating that bedforms developed in medium sand in a wide flume become 3D forms over time. The idea that persistent 2D features develop at lower flow strengths than 3D dunes (Costello & Southard, 1981; Southard & Boguchwal, 1990; Southard, 1992) does not appear valid.

There are a number of reasons as to why the discrepancy between the expected and observed morphologies may have occurred. Many of the data that have been used to design bedform phase diagrams are based on laboratory observations. The run times used in some experiments may have been too short to allow observation of the transition to 3D bedforms at lower flow strengths. Baas and collaborators suggested it might take several hours, or even several days, for the transition to occur. The reason why 3D bedforms are observed to exist in the upper part of the stability fields may simply be that it takes less time for the higher flow rate to move the sediment required for the transition.

Another possible reason why 'stable' 2D bedforms have been reported may be related to the scale of the experimental apparatus. The spanwise deformation of a bedform is certainly a function of L/y_w, where y_w is the width of the channel and L the bedform length. For example, if a dune is 1 m long in a 0·1 m wide flume, the sinuosity of the crest remains low. If a similar dune is formed in a 2 m wide flume, the crest sinuosity is free to develop. In narrow flumes, bedform three-dimensionality cannot be expressed. The 3D nature of the flow field over a bedform is also suppressed in a narrow flume. In the 1 m wide flume used for the present experiments, only the longest bedforms had $L > y_w$ and the mean eddy size (expressed by the integral time scales) is much less than the flume width (see Venditti *et al.*, 2005), so complete 3D morphology could easily be expressed.

In active sediment transport systems (rivers and tidal, nearshore and deep-water environments) frequent changes in mean hydraulics may prevent bedforms from reaching equilibrium form and thus 2D bedforms may result. Suddenly increasing the flow in the current experiments from flow strength E (0·356 m sec $^{-1}$) to A (0·501 m sec^{-1}) over a few minutes was observed to trigger a reestablishment of 2D forms. This contrasts observations by Oost & Baas (1994) who found no

return to 2D ripples in simulated tidal flow with a period of many hours. Ultimately, the development of 3D forms appears to require an extended period of steady flow.

A definition of 3D bedform morphology

Numerous researchers have examined the character of 3D dunes (reviews in Allen, 1968, 1982; Ashley, 1990), yet few have attempted to define the three-dimensionality of a bedform numerically. Allen (1968) was first to suggest a numerical measure of areal bedform morphology, defining the degree of 'waviness' of a crestline as

$$\Lambda_a = \lambda_x/\lambda_y \quad (1)$$

where λ_y is the cross-stream distance between lobes of a non-rectilinear (sinuous, catenary, linguoid, cuspate or lunate) crestline and λ_x is the streamwise distance that the lobes extend downstream (Fig. 3). A problem with Λ_a is that it suggests bedforms with oblique crestlines are 3D when, in fact, the bedforms may be straight-crested 2D forms. In a later paper, Allen (1969) suggested that bedform three-dimensionality could be characterized by the ratio (Fig. 3)

$$\Lambda_b = L/\lambda_y \quad (2)$$

and he attempted to link Λ_b functionally to a Froude number. Unfortunately, both measures suggested by Allen (1968, 1969) require rather simple bedform plan geometries. If a bedform crest is composed of multiple lobes, it becomes inordinately difficult to define λ_x and the relevant L and λ_y. In this study, in particular, the streamwise extent of lobes is not uniform along a single crestline and it is difficult to break the bedforms into individuals. It may even be misleading to break a single crestline into several paired lobes.

To demonstrate the difficulty in applying these definitions to a complex bedform field, two typically observed bedform crestline configurations are shown as examples in Fig. 3. In example 1, λ_y and λ_x can be defined allowing calculation of Λ_a, but many measurements are required to define a single bedform crest which prohibits development of a large dataset. Calculation of Λ_b is more complicated. It is fairly simple to define a bedform length for the crestline. However, the relevant length is for an individual lobe and it is not clear how to measure that length with multiple out-of-phase lobes as shown in example 1. In example 2, λ_y and λ_x can be defined, allowing calculation of Λ_a, but it is not clear that these are the most relevant length scales to define three-dimensionality. Calculation of Λ_b for example 2 is also complicated because there are multiple possible values of bedform length that can be used. These examples of typically observed crestlines show that the definition of Λ_a and Λ_b can be somewhat subjective.

In order to build a large data set of bedform three-dimensionality, a measure is defined whose components are easily obtained and not subject to the inherent subjectivity of Allen's (1968, 1969) descriptor in complex bedform fields. In this context, the non-dimensional span is defined as (Fig. 3)

$$\mathrm{NDS} = L_c/L_y \quad (3)$$

which is a simply a measure of the crest curvature or sinuosity and is akin to channel sinuosity. This measure is ideal when the crests of bedforms can be linked into a continuous crestline. Even if the bedforms are isolated individuals on the bed, NDS can be defined as L_y is measured from the ends of the crestline. As L_c and L_y are defined for the same length of crest, their combination in the parameter NDS is less subjective than Λ_a or Λ_b in a complex bedform field composed of a wide variety of deforming crestline types. NDS is insensitive to whether or not the bedform is oblique to the flow direction and is easily defined for the types of complex bedform fields observed herein (see examples in Fig. 3).

Figure 4 provides examples of NDS values averaged over the image ($\mathrm{NDS_{im}}$). When $\mathrm{NDS_{im}} = 1{\cdot}02$, the minimum observed, the bed is composed of straight-crested 2D dunes. At $\mathrm{NDS_{im}} = 1{\cdot}10$, the crestlines remain largely 2D but converge at several locations and they bend. When $\mathrm{NDS_{im}} = 1{\cdot}21$, the bed is composed of a mixture of highly sinuous and linguoid (in the terminology of Allen, 1968) bedforms. At the larger values of $\mathrm{NDS_{im}}$ in Fig. 4 (1·29 and 1·39), the bed is largely composed of linguoid bedforms with some crestlines that are highly sinuous.

These observations can be used to define a value of NDS that divides 2D dune fields from 3D fields. Instantaneously developed bedforms provide a clear transition between 2D and 3D bedforms. Bedforms that develop from bed defects in an otherwise flat bed eventually become 3D, but lag effects complicate the transition process. Therefore only the runs at greater flow

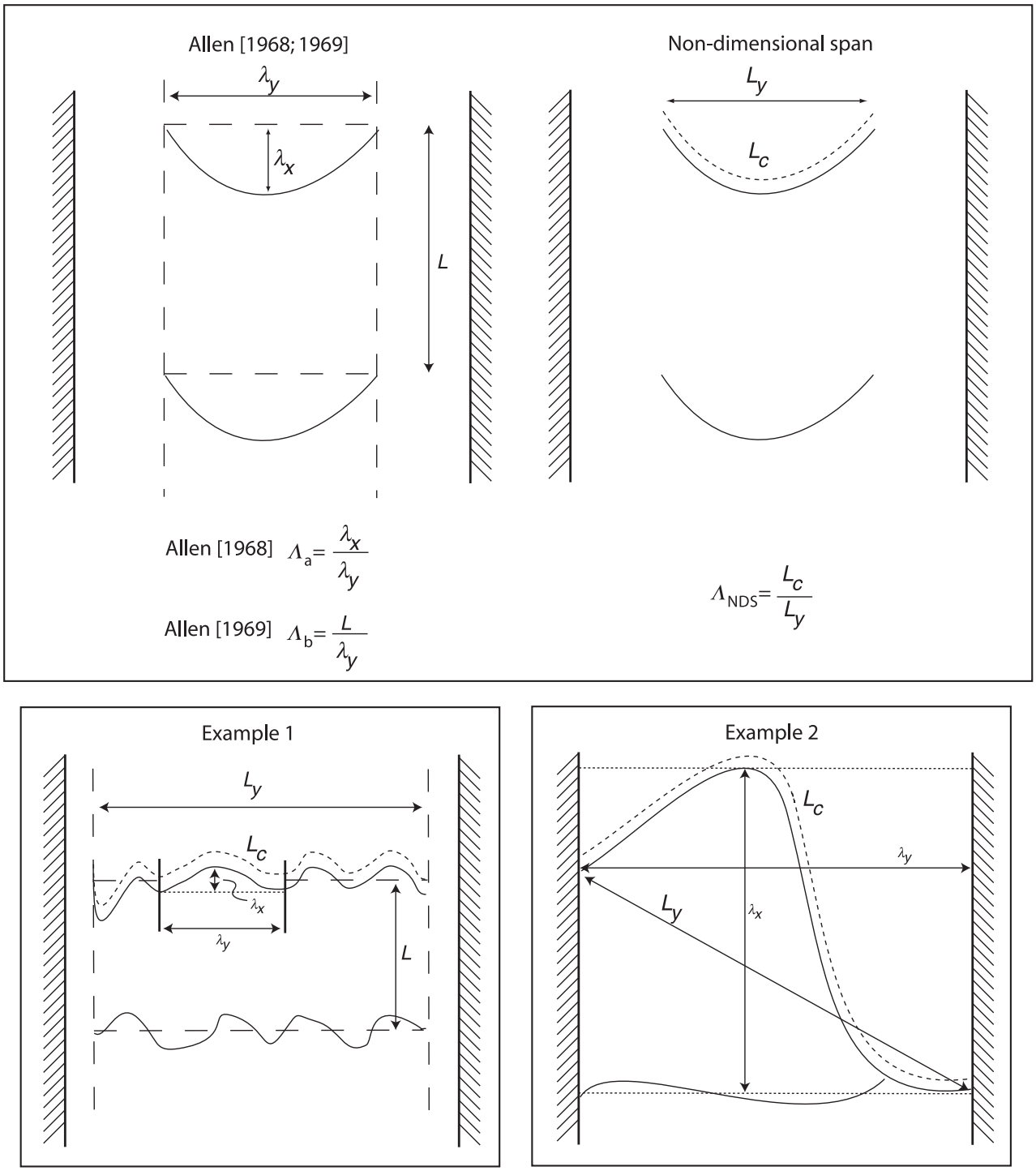

Fig. 3. Measures of bedform crestline three-dimensionality.

strengths are used to define a numerical criterion to divide 2D and 3D forms.

Figure 5 plots NDS as a function of time for the first hour of the experiments. There is considerable scatter in NDS which can be reduced by excluding values where L_y does not exceed 0·8 m (as is done in Fig. 4). Crestlines with $L_y < 0{\cdot}8$ m are generally one of the following: (i) bifurcation connector crests that join two crestlines, but are not part of the larger scale crestline shape; (ii) crestlines that are truncated at the flume walls; or (iii) fragments of crestlines that are not temporally persistent and are developed during the crestline reorientation process (see below). Generally,

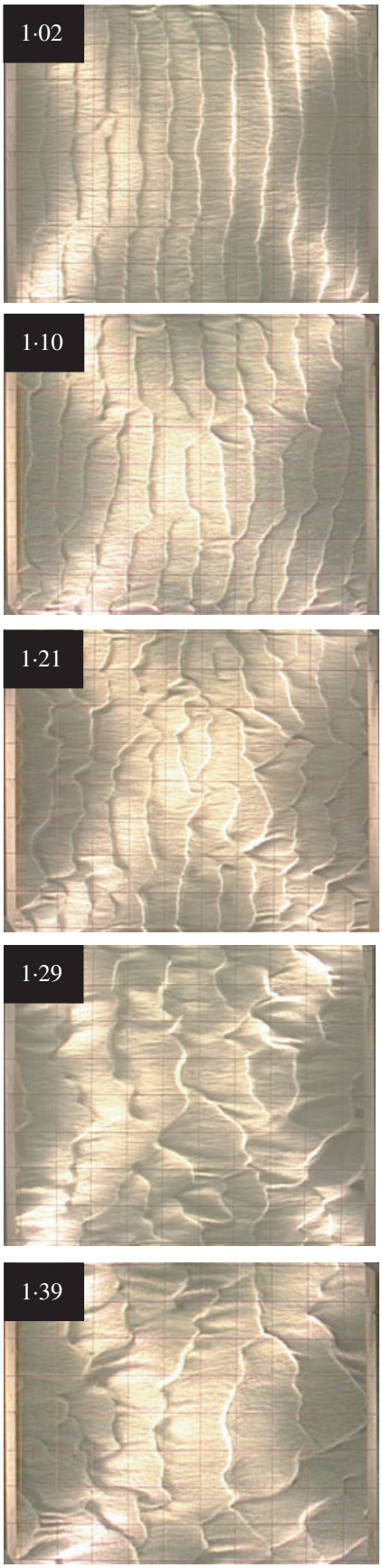

these features are not characteristic of the larger scale 3D pattern of the longer crestlines. Removing these crestlines reduces the variance in NDS revealing underlying patterns when there are many bedforms in the viewing area, but central tendencies are not strongly affected. Later in the experiments, when only 1 or 2 crestlines are observed per image, crests with $L_y < 0{\cdot}8$ m can inordinately bias the image averages (NDS_{im}).

Removing crestlines with $L_y < 0{\cdot}8$ m reveals a general trend in NDS values, but plots of NDS_{im} clarify the pattern. Initially, the majority of NDS values were in the range 1·1–1·3 with $NDS_{im} = 1{\cdot}1$–$1{\cdot}2$ when the bed was composed of organizing perturbations (see Venditti *et al.*, 2005 for discussion of this organization process). As the crestlines developed from these perturbations and became 2D, NDS_{im} began to drop, approaching its definitional minimum of 1·0.

At flow strength B, crestlines that were continuous across the channel formed at $t_c = 120$ sec, while minimum values of NDS occurred at $t_{2D} = 420$ sec, *ca* 5 min later (Table 2). Similar trends were observed at flow strengths A and C where $t_{2D} - t_c \approx 300$ sec. This timing appears not to depend on flow strength, although the range of flow strengths is rather narrow for such a conclusion. At t_{2D} there were several observations of NDS $\approx 1{\cdot}00$, but $NDS_{im} = 1{\cdot}02$, 1·08 and 1·07 at flows A, B and C respectively. NDS_{im} was much lower at flow strength A, but this observation could be fortuitous as lower values of NDS_{im} may have occurred in between the sampled images at flows B and C.

Roughly 10–30 min beyond the minimum, NDS_{im} increases to values that are as large as 1·38–1·39 (Fig. 5). There is a nearly linear increase in NDS_{im} from 1·02 to 1·39 at flow A, after which NDS_{im} varies between 1·2 and 1·4 as the bedforms grew towards an equilibrium. The same near-linear increase was observed at flows B and C, but from $NDS_{im} = 1{\cdot}07$ to 1·29 and from 1·08 to 1·31, after which NDS_{im} approaches 1·4.

Figure 5 demonstrates that, as crestlines begin to break up and become 3D, NDS rose until more than 80% of all observations with $L_y > 0{\cdot}8$ m were above a value of 1·2. The scatter about NDS_{im} also

Fig. 4. Examples of non-dimensional span averaged over each image. From top to bottom, images are from flow A at $t = 300$ sec, flow B at $t = 660$ sec, flow C at $t = 1020$ sec, flow B at $t = 2160$ sec and flow A at $t = 1680$ sec. Grid spacing is 0·115 m and flow is from left to right.

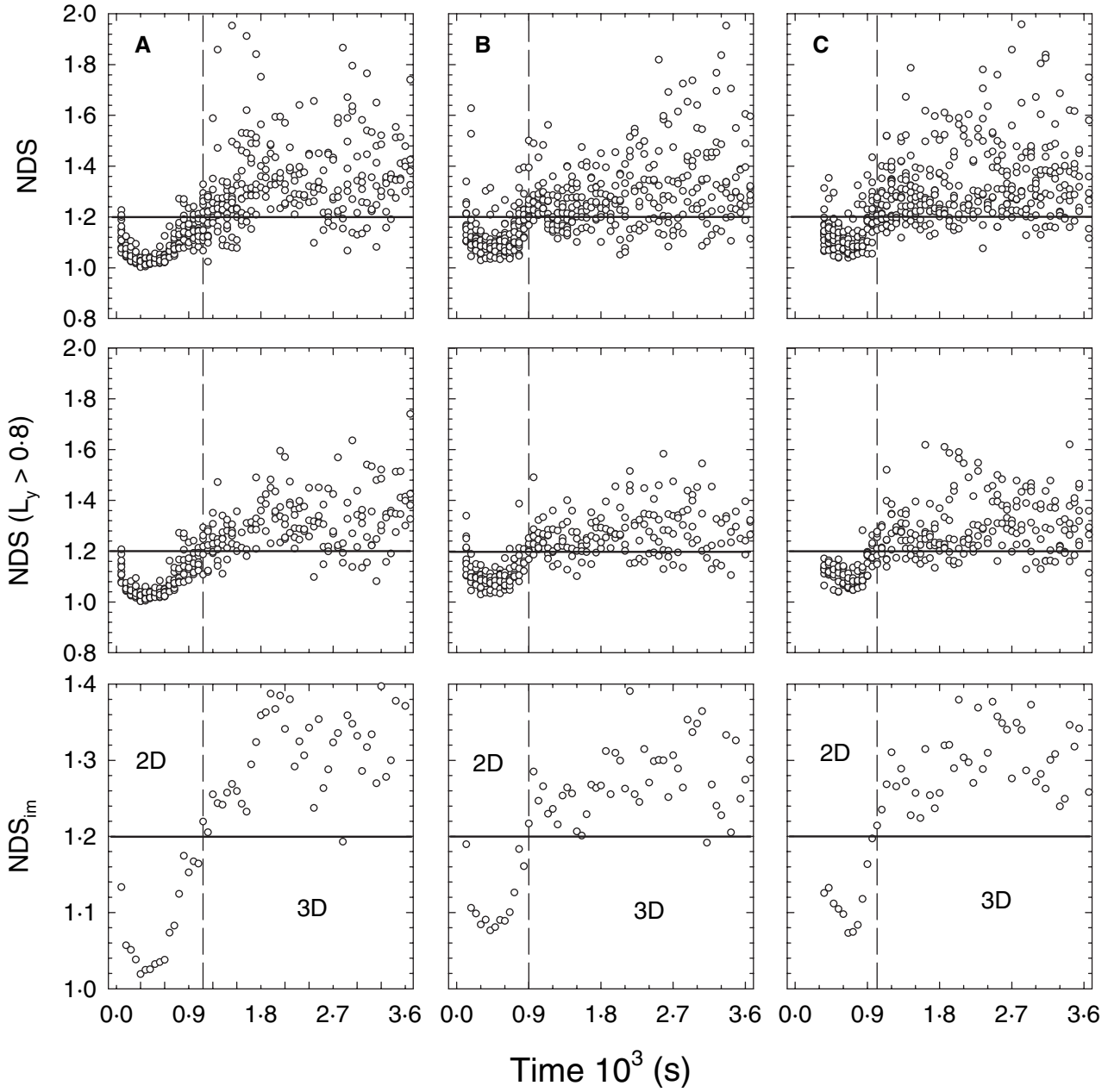

Fig. 5. Non-dimensional span (NDS) during the first hour of experiments. All observations are plotted in top row of panels. Middle panels plot crests that exceed a cross-stream extent of 0·8 m and bottom panels are image means of data in middle row. A, B and C denote experimental runs.

Flow	t_c (sec)	NDS_{im}	t_{2D} (sec)	NDS_{im}	t_{3D} (sec)	NDS_{im}
A	60	1·1332	300	1·0192	1080	1·2195
B	120	1·1895	420	1·0764	900	1·2169
C	360	1·1256	660	1·0730	1020	1·2141

Table 2. Timing of critical non-dimensional span values during the hour of the experiments as the 2D–3D transition occurs.

increased substantially compared to when NDS is <1·2 because the bed was composed of bedforms with varying degrees of three-dimensionality. Given these observations and the description associated with $NDS_{im} = 1·21$ in Fig. 4, it seems logical to assert that when NDS is <1·20 a

crestline is 2D, and when NDS exceeds 1·20 a crestline is 3D. The experimental time when NDS_{im} first exceeds 1·2 (t_{3D}) is essentially unchanged across the limited range of flow strengths examined here (Table 2).

Bedform growth and variation in the non-dimensional span

Echo-sounder data reveal how bedform height H, length L and migration rate R evolved as a function of time (Fig. 6). Initial bedform heights were a few millimetres while initial lengths were 30–100 mm. Regardless of whether the bedforms were initiated instantaneously or by defects, bedforms grew in H and L while R decreased towards equilibrium values. Bedform growth was approximately exponential and can be expressed by

$$H = a_H\left(1 - e^{-b_H \cdot t}\right) \quad (4)$$

$$L = a_L\left(1 - e^{-b_L \cdot t}\right) \quad (5)$$

where a_H, a_L, b_H and b_L are coefficients derived from least-squares regression through time series plotted as in Fig. 6. Bedform migration rates decrease exponentially with time and can be expressed by

$$R = a_R e^{(b_R/(t+c_R))} \quad (6)$$

where a_R, b_R, and c_R are least-squares regression coefficients. Values for a, b, and c are given in Table 3. No substantial change in migration rate was observed at flow E, so Eq. (6) is not applicable. All model fits are significant at the 95% confidence interval, but more bedforms are observed in the runs with larger flow strengths and consequently the model fit is better (see r^2 values).

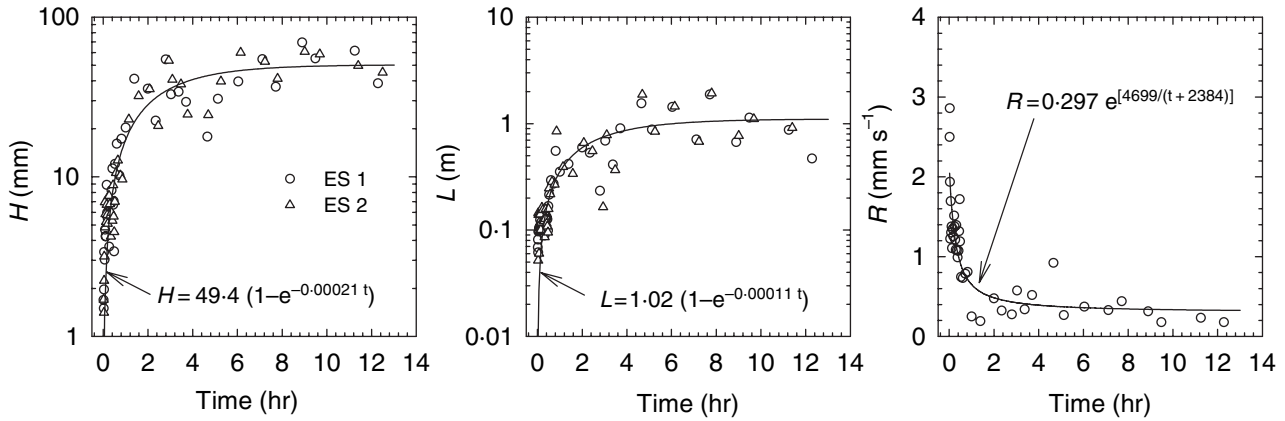

Fig. 6. Typical bedform growth curves for height H, length L and migration rate R. Data are drawn from echo-sounders at flow B. Data for flows A, C, D and E can be found in Venditti (2003). ES 1 and ES 2 refer to echo-sounders 1 and 2. Time t is in seconds for model fit of Eqs (4), (5) and (6).

Table 3. Model-fitting results.

Value	Flow A	Flow B	Flow C	Flow D	Flow E
a_H, mm	50·36	49·36	43·54	22·2	20·5
b_H, 10^{-4}	1·147	2·113	1·12	2·455	2·211
r_H^2	0·84	0·82	0·84	0·4	0·29
p_H	< 0·0001	< 0·0001	< 0·0001	< 0·0001	0·0013
a_L, m	1·208	1·017	1·244	0·411	0·32
b_L, 10^{-4}	1·798	1·068	0·959	2·386	1·563
r_L^2	0·31	0·67	0·69	0·21	0·18
p_L	< 0·0001	< 0·0001	< 0·0001	0·0026	0·016
a_R, mm sec^{-1}	0·566	0·297	0·253	0·135	n/a
b_R	2416	4699	4593	5118	n/a
c_R	1422	2384	3032	4411	n/a
r_R^2	0·8	0·78	0·84	0·52	n/a
p_R	< 0·0001	< 0·0001	< 0·0001	0·0014	n/a

Time t is in seconds in Eqs (4), (5), and (6).

The time required to reach equilibrium bedform dimensions T_e was determined when the exponential curve visually approached its asymptote (a_H or a_L). Defined in this manner, T_e is approximately 1·5–3 h (Table 4). Baas (1994) defined T_e when exponential functions similar to Eqs (4) and (5) reached 99% of their asymptote, but this criterion could not be used here as some best-fit regressions did not reach a true asymptote. Reducing this limit to 90% of the asymptote produces values that are similar to those based on visual inspection (i.e. later than 1·5–3 h; Table 4). Statistical equilibrium, as defined by Baas (1994), does not occur until later in the experiments. Baas and collaborators (Baas *et al.*, 1993; Baas, 1994, 1999) observed an increase in T_e with decreasing flow velocity. No pattern in T_e was observed with flow strength, but the flows are sufficiently similar that generalizations are not warranted.

The 2D–3D transition occurred during the exponential increase in bedform size, well before the apparent onset of the equilibrium phase. Figure 7 shows changes in NDS_{im} as the bedforms evolved over the entire experiment. As the bedforms grew, there was a clear increase in NDS_{im} but it is not clear if the increase in bedform size is directly linked to bedform three-dimensionality in a mechanistic fashion. In order to examine this, fluctuation in NDS_{im} during the equilibrium stage needs to be examined.

The most detailed NDS record was generated for flow B, in which there is clear evidence of at least two dramatic increases in the three-dimensionality of the bedforms in the video view, separated by *ca* 4·5 h, at 5·5 and 10 h. Local periodic return to sinuous ripples in steady flow which resulted in quasi-periodic variation of bedform length and height was also observed by Baas (1999). There is no relevant time-scale associated with the flow or the flume that might cause this. However, low relief bars are known to develop in flumes (Bennett & Bridge, 1995). It is easy to envision a scenario that might lead to changes in the flow velocity and depth as a bar form passes that could account for the abrupt increase in NDS_{im}.

Changes in the mean equilibrium-phase bedforms properties (H, L, R) are not coupled with changes in the mean equilibrium stage NDS. Based on echo-soundings, mean equilibrium-stage heights $\bar{H}_e$ range between 20 and 48 mm, lengths $\bar{L}_e$ range between 0·30 and 1·17 m and migration rates $\bar{R}_e$ range between 0·1 and 0·6 mm sec^{-1}. $\bar{H}_e$, $\bar{L}_e$ and $\bar{R}_e$ increased with flow strength (Table 1). In contrast, $\overline{NDS}_{im}$ did not display any relation to flow strength (Table 1). Furthermore, Fig. 7 indicates that NDS_{im} exits its growth phase well before equilibrium heights and lengths are achieved.

Figure 8 displays the relation between bedform size and its three-dimensionality by plotting NDS_{im} against bedform length measured from the video. There seems to be a near linear increase in NDS_{im} when the bedforms are small ($L_a < 0{\cdot}15$ m), but this is because NDS and L_a are both undergoing a near linear increase with time as the initial 2D–3D transition occurs. After the initial transition, when the bedforms are growing and large, during the pattern equilibrium stage ($L_a < 0{\cdot}15$ m), there does not appear to be any relation between L_a and NDS. This implies that there is not a limiting bedform size (H or L) for 2D dunes in the experiments and that there is no change in height or length that triggers the transition to 3D morphology. However, variation in these parameters may be too great to recognize a relation.

PROCESS OF THE 2D TO 3D BEDFORM TRANSITION

At low flows (flows D and E), sediment transport remains low, so the 2D–3D transition in

Table 4. Time to equilibrium using various methods; all values in hours.

Value	Flow A	Flow B	Flow C	Flow D	Flow E
Visual estimate of when curve approaches asymptote					
T_e (H or L)	1·5–3·0	1·5–3·0	1·5–3·0	1·5–3·0	1·5–3·0
When H or L first exceeds a_H or a_L					
$T_e(H)$; $H > a_H$	2·0	2·8	1·5	1·5	1·8
$T_e(L)$; $L > a_L$	2·0	4·7	3·4	1·3	2·3
Baas (1994) method with various thresholds					
T_e; $H = 0{\cdot}99a_H$	11·2	6·1	11·2	5·1	5·6
$T_e(L)$; $L = 0{\cdot}99a_L$	7·1	> 12 h	> 12 h	5·3	8·1
T_e; $H = 0{\cdot}90a_H$	5·6	3·1	5·8	2·7	2·9
$T_e(L)$; $L = 0{\cdot}90a_L$	3·6	6·0	6·8	2·8	4·1

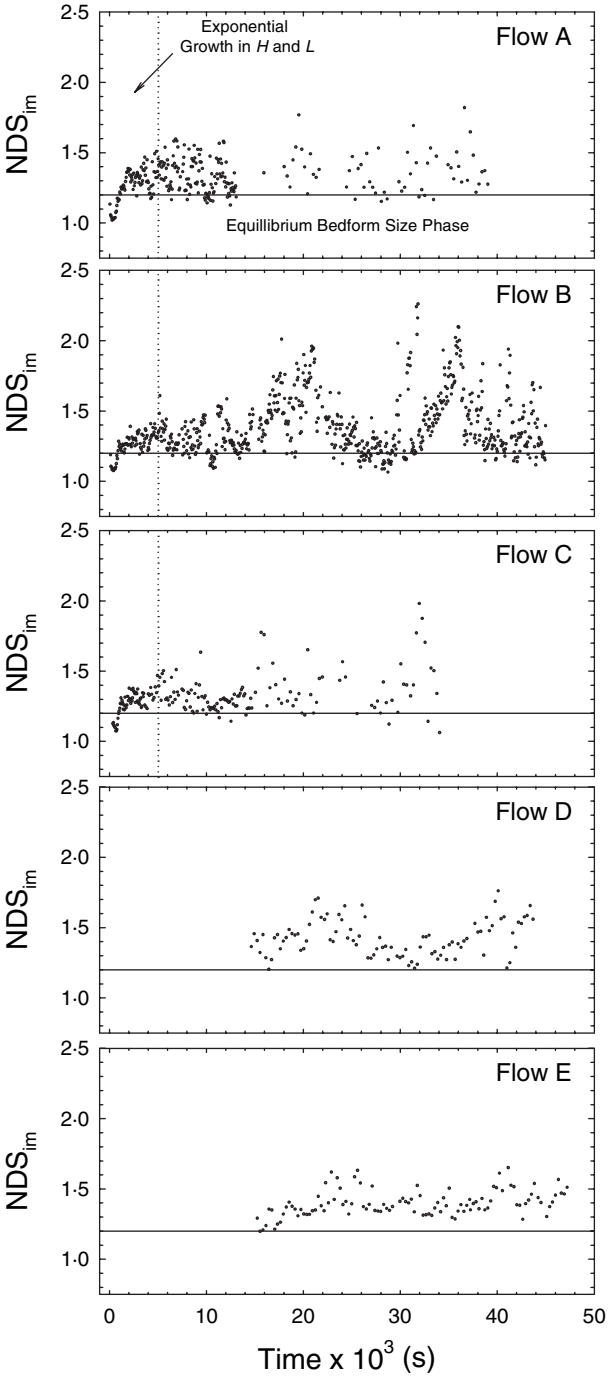

Fig. 7. Image averaged non-dimensional span NDS_{im} time series. NDS_{im} includes those crests whose cross-stream extent exceeds 0·8 m. The vertical dashed line divides the period of exponential bedform growth from the equilibrium phase at 5000 sec.

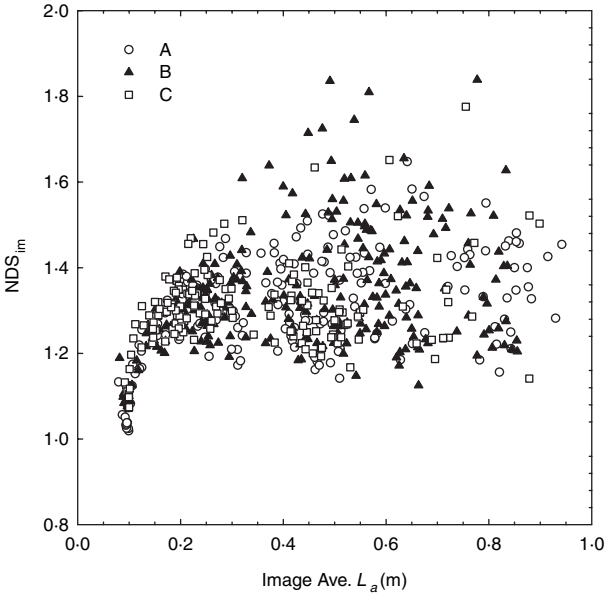

Fig. 8. Image averaged non-dimensional span NDS_{im} plotted against areally averaged bedform length L_a for flows A, B and C. NDS_{im} includes those crests whose cross-stream extent exceeds 0·8 m.

defect-developed dune trains is slow and the transition time is ambiguous. The transition is pronounced at higher flows when the bedforms are developed instantaneously from an initially flat bed. Figure 9 depicts a series of morphological changes that the 2D bed undergoes during the transition to 3D when the bed is developed instantaneously. Once organized into bedforms, the bed is composed of straight or slightly sinuous crested dune features (Fig. 9A). The crestlines begin to bend along their cross-stream length and become convex downstream during the greatest flow strength examined (A) (Fig. 9B). At flow B bending is less perceptible, and does not occur at flow C, the lowest instantaneous initiation flow strength. Presumably, this phenomenon is caused by side wall drag, where the wall fluid is moving slightly slower compared to fluid in the centre of the flume. The cross-stream gradient is strongest at the greatest flow strengths.

As the 2D bed (and 2D bed with bending crests) persists, crest defects sporadically form, which are minor, transient excesses or deficiencies of sand in the crestline. Figure 10A shows several crest defects developed in the 2D field that appear similar to dune blowouts observed along coastal sand dunes formed by sea breezes (Hesp & Hyde, 1996). Crest defect development may be linked to turbulent bursting over the 2D bed, but the measurements taken herein are inappropriate to test this hypothesis.

Crest defect features are passed from crest to crest and can be seen to migrate though the dune field (Fig. 10B). When the defect is formed a

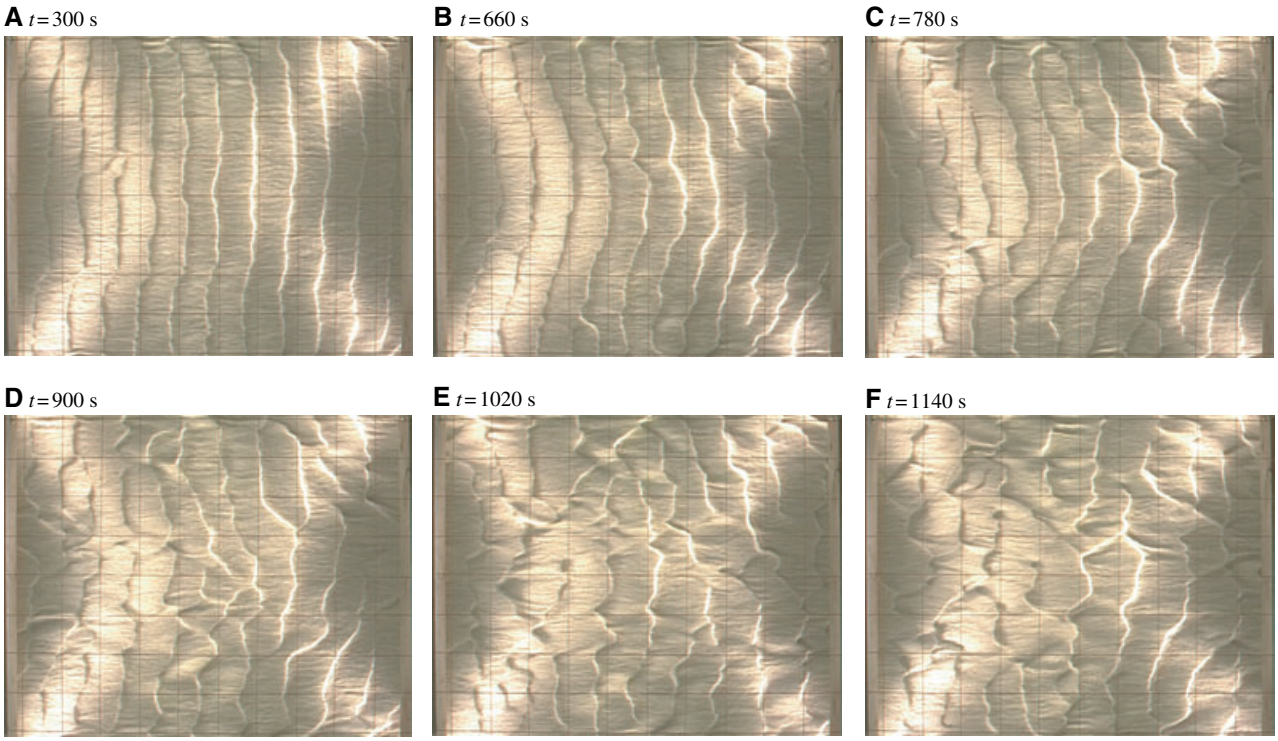

Fig. 9. Transition between instantaneously initiated 2D and 3D dunes at flow strength A. Grid spacing is 0·115 m and flow is from left to right.

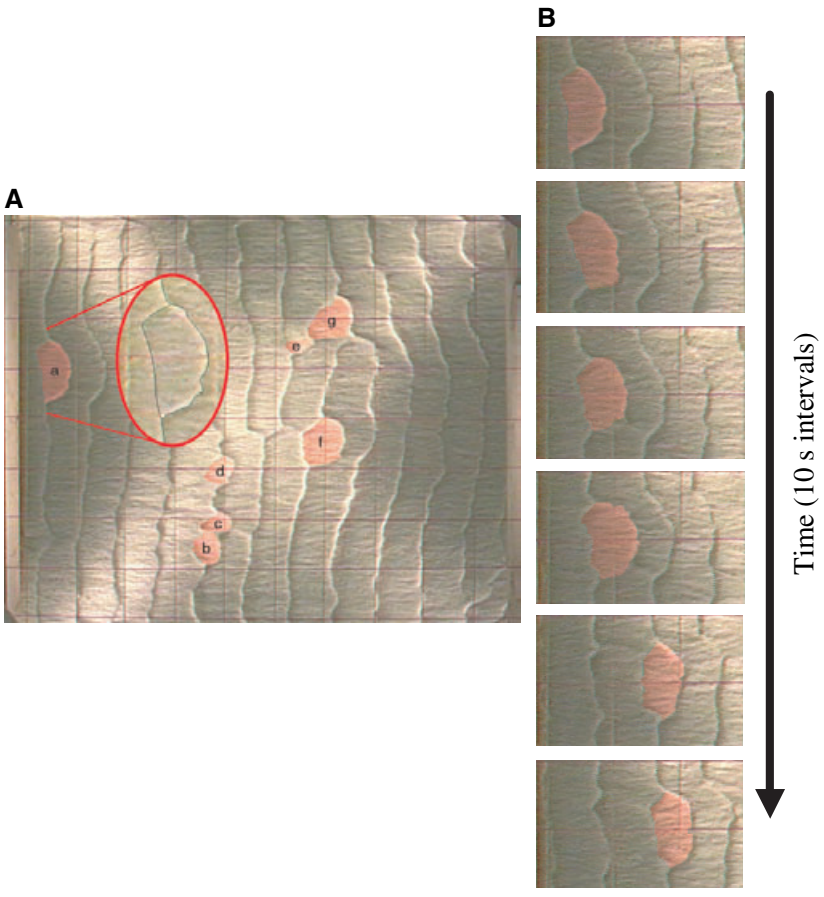

Fig. 10. (A) Crest defects developed during flow B at $t = 320$ sec. $NDS_{im} \approx 1{\cdot}1$. The area in the red oval is defect 'a' magnified by 200%. (B) Progression of defect 'a' from panel (A) as it migrates from one crest to the next ($t = 320$–370 sec). The area highlighted red is the parcel of sand passed from one crest to another. Note the effect of defect progression on the downstream crest before it cleaves from the upstream crestline. Grid spacing is 0·115 m and flow is from left to right.

volume of sediment is generated downstream causing a convex downstream bulge in the crestline in-line with the defect. The parcel of sand that composes the defect is elongated downstream, flattening it. The dune crestline acts as a barrier to flow. Once the barrier is reduced in the form of a crest defect, the downstream crestline is exposed to a greater flow velocity than the rest of the downstream crest and another blowout is formed in line with the previous defect. The defect sand parcel is thus cleaved from the crestline and passed to the downstream crest.

Crest defect features move through the bedform field at a velocity *ca* 2× the dune migration rate. The defects in Fig. 10A moved at an average rate of 2·9 mm sec^{-1} while the bedforms moved at only 1·5 mm sec^{-1}. The larger defects, such as A and F, moved through the dune field more quickly than the others, with velocities of 3·6 and 3·5 mm sec^{-1} respectively. Smaller defects, such as D and B, moved at a velocity of 2·5 mm sec^{-1}.

Crest defects are of little consequence when the bed is composed of straight or slightly sinuous dunes. Defects are successfully passed from one crestline to the next without altering the morphological characteristics of the crest (Fig. 10B) and the non-dimensional span remains below 1·2. Crest defects are generally passed through a few crestlines and then disappear when the bed is 2D and so the field appears able to absorb a limited number of defects. However, the number of crest defects increases with time and the 2D field is eventually overwhelmed (Fig. 9C and D). The non-dimensional span increases to above 1·2. When this occurs, crest defects slow their downstream march and eventually stop, causing permanent changes in the crestline (Fig. 9E and F). The defects interact and the bed falls into a stage where the 3D bed is maintained indefinitely.

Operation and maintenance of the 3D bed

Allen (1973) provided a description of the mechanisms associated with the development and modification of a 3D bed that Baas (1994) aptly called ripple 'birth-and-death processes'. On the basis of observations made mainly in a 2D streamwise vertical plane, Allen (1973) indicated that new ripples may be developed by a crestline splitting along its cross-stream length at spurs, which are ridges of sand on dune backs perpendicular to crestlines. Alternatively, a new ripple of limited height may be generated on an existing ripple back that grows in height and splits the original ripple length. Death occurs by a number of different processes. Rapid deceleration of a ripple can occur if the crestline becomes strongly concave downstream which leads to a concentration of the lee side vortex and a deep scour pit. The increased erosion accelerates the next crest's downstream migration, starving crests further downstream of material and allowing the accelerating ripple to overtake the downstream ripples. Increasing the local height of a ripple may also lead to downstream features being planed off, and one or more crestlines being destroyed by the efficiency of the separation vortex.

Allen (1973) noted that all these processes are at work on the bed at any one time, but only in exceptional cases do they lead to the generation or extinction of a ripple. Our observations indicate that while these processes are observed in a 2D plane, they are a secondary manifestation of the dominant process – the growth of crestline lobes – observed to maintain the 3D bed. Maintenance is achieved by the constant rearrangement of crestlines by lobe extension and growth and local scour development associated with saddle-shaped crestlines.

Lobe extension (Fig. 11) is caused by localized increases in bedform height across the flume and erosion of a scour pit in the lee of the bedform. As the increased available sediment extends the lobe, it will sometimes stop and be planed out. Frequently, the lobe will begin to locally starve the downstream crestline of sediment while the rest of that crestline continues to move (Fig. 11B). Eventually, the upstream and downstream crestlines will meet and two fragments will join (Fig. 11C), forming a new crestline and two bifurcations (Fig. 11D). Concurrent with this process, local crestline heights are increased in downstream dunes, forcing new crest lobe growth downstream. As long as H and L vary across the channel, this process of lobe extension continues to maintain the 3D bed. Once the bed becomes 3D it cannot become 2D again without some external trigger, such as a change in flow rate. As noted above, when the flow rate was increased, 2D dunes briefly re-established themselves, but became 3D a short time later. In summary, there is a constant rearranging of crestlines that gives the appearance of the birth and death process described by Allen in the streamwise plane.

Raudkivi & Witte (1990) have previously suggested that bedforms actually grow in length through the birth and death cycle by the coalescence of smaller bedforms, because smaller bedforms have larger migration rates and can

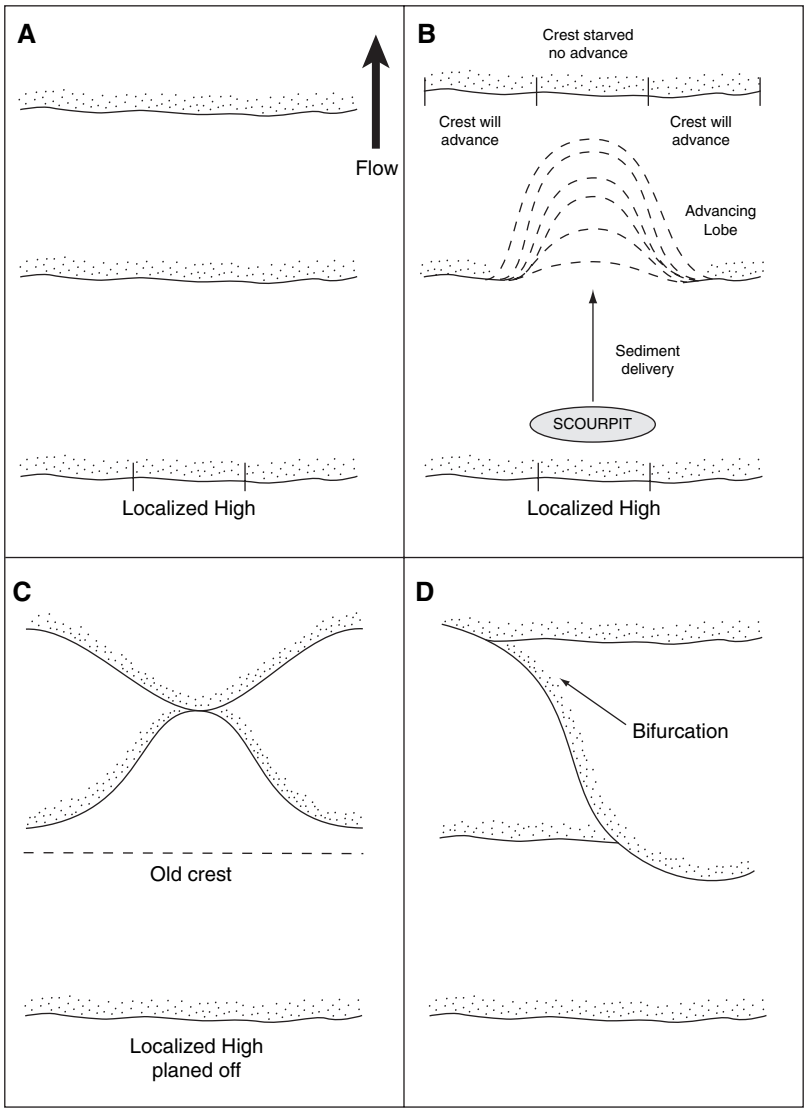

Fig. 11. Schematic of an advancing crestline lobe as it joins with the downstream crestline and generates bifurcations.

overtake the larger features on a bed. Coleman & Melville (1994) have shown a relation between bedform size and migration velocity, albeit in a narrow flume where bedform three-dimensionality is suppressed. Ditchfield & Best (1990) argued against bedform growth solely by coalescence indicating that there is no relation between bedform size and the migration rate. They also suggested that bedforms may both grow or attenuate without interaction with other bedforms, or alternatively, they may coalesce as they migrate.

Contrary to Ditchfield & Best (1990), a strong nonlinear relation was observed between image averaged L and R (Fig. 12), and seems reasonably to be expected because of the changing mass transfer requirement to displace dunes of different size. Nevertheless, what bedform coalescence was observed during the experiments was limited to thin migrating sand sheets on the dune stoss reaching the crestline and avalanching into the dune lee (Venditti *et al.*, in press). This was an equilibrium process that maintained transport over the dune but did not cause dune growth. Widespread bedform coalescence, as is suggested in bedform unification models (Raudkivi & Witte, 1990), did not occur amongst the dune population either during the growth or equilibrium phases. Rather, crest realignment by the growth of scour-induced crest lobes dominated, often giving the appearance of bedform coalescence in the 2D streamwise vertical plane.

Consideration of bedform kinematics suggests that, without bedform coalescence, slow stretching of the bedform field by a subtle downstream acceleration of bedforms is required to accommodate the temporal deceleration during the

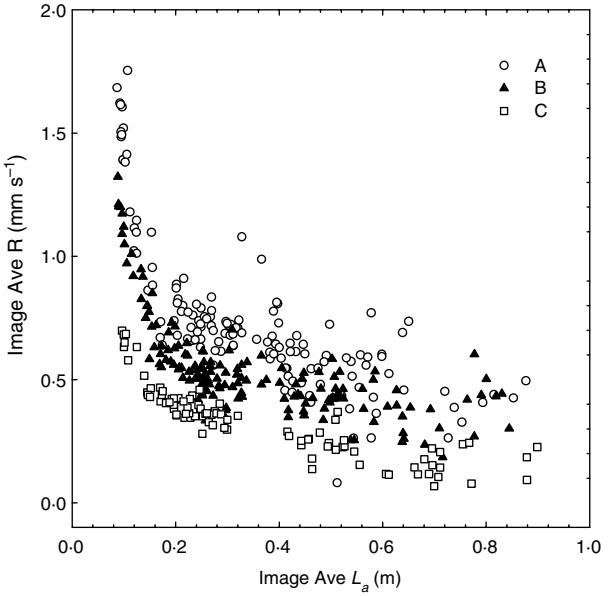

Fig. 12. Relation between bedform length L and migration rate R measured from the video. Values have been averaged over a bedform crestline and then averaged over an image. There is a practical limit of *ca* 1·2 m on the measured lengths because that is the size of the observing window.

bedform growth phase, but the acceleration occurs with a cross-stream vector in a 3D bedform field. It is likely that acceleration and deceleration of bedforms over bars and through bends dominate the bedform growth and abatement mechanism in natural channels. Models of bed roughness evolution that consider bedform three-dimensionality as a secondary descriptor of a bedform field or an ancillary property may be inadequate descriptions of the process.

SUMMARY AND CONCLUSIONS

Experiments conducted in a 1 m wide flume using a narrowly graded, 500 μm size sand subjected to a 0·15 m deep, non-varying mean flow ranging from 0·30 to 0·55 m sec^{-1} reveal a transition between the initial 2D bedforms and 3D bedforms. This is an interesting observation because conventional bedform phase diagrams suggest that 2D dune fields should be formed under these hydraulic conditions. That stable 2D dunes were not observed in this calibre sand calls into question the reliability of bedform phase diagrams using crestline shape as a discriminator. These results confirm the work of Baas and collaborators (Baas *et al.*, 1993; Baas, 1994, 1999) who suggested that the 2D–3D transition is inevitable on a rippled bed if a flow persists for a sufficiently long period. Our observations suggest that this is also the case for larger scale dune bedforms.

Statistics of the planimetric bed morphology reveal that bedforms become three-dimensional when the crest non-dimensional span (sinuosity) becomes >1·2. The significant variation observed in the non-dimensional span cannot be linked to systematic variation in the bedform size and does not apparently increase with flow strength. There is no obvious limiting bedform size (height or length) for 2D dunes in the experiments nor is there a change in height or length that appears to trigger the transition to 3D morphology. Thus, bedform three-dimensionality seems to be an inherent property of deforming channel beds.

The transition between 2D and 3D bedforms appears to be linked to defects developed in the bedform crestline. Video images reveal that, once 2D bedforms are established, minor, transient excesses or deficiencies of sand are passed from one crestline to another. The bedform field appears capable of absorbing a small number of such defects but, as the number grows with time, the resulting morphological perturbations produce a transition in bed state to 3D forms that continue to evolve, but are pattern-stable. The 3D pattern is maintained by the constant rearrangement of crestlines through lobe extension, starving downstream bedforms of sediment, which leads to bifurcation. Widespread bedform coalescence did not occur amongst the dune population. Rather, crest realignment by the growth of scour induced crest lobes dominated, often giving the appearance of bedform coalescence in the 2D streamwise vertical plane.

Bedform growth occurred without extensive coalescence of smaller features as suggested in bedform unification models (i.e. Raudkivi & Witte, 1990; Coleman & Melville, 1994). However, a nonlinear relation between bedform size and migration rate shows that the smaller features move more quickly. Bedform kinematics suggest that, for this to occur, a spatial acceleration of the bedforms is required to accommodate the temporal deceleration of bedforms as they get larger without widespread coalescence. In a 3D bedform field, some portion of that acceleration is accommodated by the cross-stream crest realignment process, suggesting that models of bed roughness evolution which consider bedform three-dimensionality as a secondary descriptor of a bedform field or an ancillary property may be inadequate descriptions of the growth process.

ACKNOWLEDGEMENTS

Financial support to JV came through a University Graduate Fellowship, a Natural Science and Engineering Research Council of Canada (NSERC) Post-Graduate Scholarship and a Research Assistantship provided through a Natural Science and Engineering Research Council of Canada Discovery Grant to MC. Funds for the experiments were provided by the U.S. Department of Agriculture and the NSERC grant. The video image frame grabber was purchased using a Ph.D. Research Grant from the Association of American Geographers – Geomorphology Speciality Group. N. Manklow and C. Christie were largely responsible for digitising the bedforms from the image sequences and assisted with the analysis of the echo-soundings. Their patience and good humour are greatly appreciated. J. Cox, J. Milam, and D. Wren at the USDA-ARS and V. Kujala at UBC provided technical support. Comments made by J. Southard, J. Baas and an anonymous journal reviewer were greatly appreciated.

NOMENCLATURE

A_b Planimetric bedform area
d Flow depth
D, D_{50} Grain size and its median
ff Friction factor
Fr Froude number
g Gravitational acceleration
H, H_e Dune height and its equilibrium value
L, L_e Dune length and its equilibrium value
L_a Areal bedform length
L_c Distance along bedform crest
L_y Linear distance between the end points of the crestline
Q Discharge
R, R_e Dune migration rate and its equilibrium value
Re, Re_g Reynolds number and grain Reynolds number
S Water surface slope
t Time or experimental time
t_{2D} Time to the development of 2D bedforms
t_{3D} Time to the development of 3D bedforms
t_c Time to when bedforms extend across the channel
T_e Time to equilibrium height and length
u_* Shear velocity
$\bar{U}$ Mean flow velocity
y_b Distance that bedform extended across flume
y_w Flume width
λ_x Streamwise distance lobes of three-dimensional bedforms extend downstream
λ_y Cross-stream distance between lobes of a three-dimensional bedform
Λ_a, Λ_b Measures of bedform three-dimensionality
NDS, NDS_{im} non-dimensional span and its image average
ν Kinematic viscosity of water
ρ Density of water
τ shear stress.

REFERENCES

Allen, J.R.L. (1968) *Current Ripples*. North Holland Publishing Company, Amsterdam, 433 pp.

Allen, J.R.L. (1969) Some recent advances in the physics of sedimentation. *Proc. Geol. Assoc.*, **80,** 1–42.

Allen, J.R.L. (1973) Features of cross-stratified units due to random and other changes in bed forms. *Sedimentology*, **20,** 189–202.

Allen, J.R.L. (1982) *Sedimentary Structures: Their Character and Physical Basis*. Elsevier Science Publishers, New York.

Ashley, G.M. (1990) Classification of large-scale subaqueous bedforms: a new look at an old problem. *J. Sed. Petrol.*, **60,** 160–172.

Baas, J.H. (1994) A flume study on the development and equilibrium morphology of current ripples in very fine sand. *Sedimentology*, **41,** 185–209.

Baas, J.H. (1999) An empirical model for the development and equilibrium morphology of current ripples in fine sand. *Sedimentology*, **46,** 123–138.

Baas, J.H., Oost, A.P., Sztano, O.K., de Boer, P.L. and **Postma, G.** (1993) Time as an independent variable for current ripples developing towards linguoid equilibrium morphology. *Terra Nova*, **5,** 29–35.

Bennett, S.J. and **Bridge, J.S.** (1995) The geometry and dynamics of low-relief bed forms in heterogeneous material in a laboratory channel, and their relationship to water flow and sediment transport. *J. Sed. Res.*, **A65,** 29–39.

Coleman, S.E. and **Melville, B.W.** (1994) Bed-form development. *J. Hydraul. Eng.*, **120,** 544–560.

Costello, W.R. and **Southard, J.B.** (1981) Flume experiments on lower-regime bedforms in coarse sands. *J. Sed. Petrol.*, **51,** 849–864.

Ditchfield, R. and **Best, J.L.** (1990) Development of bed features: discussion. *J. Hydraul. Eng.*, **116,** 647–650.

Guy, H.P., Simons, D.B. and **Richardson, E.V.** (1966) Summary of alluvial channel data from flume experiments, 1956–1961. *US Geol. Surv. Prof. Pap.*, **462-I,** 1–96.

Hesp, P.A. and **Hyde, R.** (1996) Flow dynamics and geomorphology of a trough blowout. *Sedimentology*, **43,** 505–525.

Oost, A.P. and **Baas, J.H.** (1994) The development of small scale bedforms in tidal environments: an empirical model for unsteady flow and its applications. *Sedimentology*, **41,** 883–903.

Raudkivi, A.J. and **Witte, H.-H.** (1990) Development of bed features. *J. Hydraul. Eng.*, **116,** 1063–1079.

Simons, D.B. and **Richardson, E.V.** (1966) Resistance to flow in alluvial channels. *US Geol. Surv. Prof. Pap.*, **422-J,** 1–61.

Simons, D.B., Richardson, E.V. and **Albertson, M.L.** (1961) Flume studies using medium sand (0.45 mm). *US Geol. Surv. Prof. Pap.*, **1498-A,** 1–76.

Southard, J.B. (1992) *Interpreting Primary Physical Bedding Structures: A Short Course given at the University of Southern California*. University of Southern California, Los Angeles, CA.

Southard, J.B. and **Boguchwal, L.A.** (1990) Bed configurations in steady unidirectional water flow part 2. Synthesis of flume data. *J. Sed. Petrol.*, **60,** 658–679.

Venditti, J.G. (2003) *The initiation and development of sand dunes in river channels*. PhD thesis, The University of British Columbia, Vancouver.

Venditti, J.G., Church, M.A. and **Bennett, S.J.** (2005) Bed form initiation from a flat sand bed. *J. Geophys. Res.*, **110,** doi:10.1029/2004JF000149.

Venditti, J.G., Church, M.A. and **Bennett, S.J.** (in press) Morphodynamics of small-scale superimposed sandwaves over migrating dune bedforms. *Water Resour. Res.*.

Manuscript received 5 August 2004; revision accepted 20 July 2005.